

DRAFT

1
2
3
4
5
6
7
8
9
10
11
12
13
14
15
16
17
18
19
20
21
22
23
24
25
26
27
28
29

Evaluation of Pressurizer Alloy 82/182 Nozzle Failure Probability

(Including Effect of the Fall-06 Wolf Creek NDE Indications)

Peter C. Riccardella
Dilip Dedhia
David O. Harris

Structural Integrity Associates, Inc.

July 14, 2007

DRAFT

Table of Contents

1		
2		
3		
4	1.0	Introduction
5		
6	2.0	Flaw Distributions
7		
8	2.1	Inspection Data
9	2.2	Statistical Fits to the Data
10		
11		
12	3.0	Critical Flaw Size Distribution
13		
14	3.1	Applied Load Distribution
15	3.2	Compilation of Full Scale Pipe Tests
16	3.3	Development of Fragility Curve
17		
18	4.0	Crack Growth
19		
20	4.1	Summary of Advanced FEA Results
21	4.2	Adaptation to Probabilistic Analysis
22		
23	5.0	Monte Carlo Analysis
24		
25	5.1	Methodology
26	5.2	Cases Analyzed
27	5.3	Results
28		
29	6.0	Conclusions
30		

DRAFT

1 Introduction

To complement the deterministic analyses being performed under the advanced FEA project [1], the MRP also performed a probabilistic evaluation of the Alloy 82/182 pressurizer butt welded nozzles, considering current inspection data, to assess the effect of various inspection options on probability of a nozzle failure in the time interval until all nozzles are inspected or mitigated. There are three major elements to the probabilistic analysis approach:

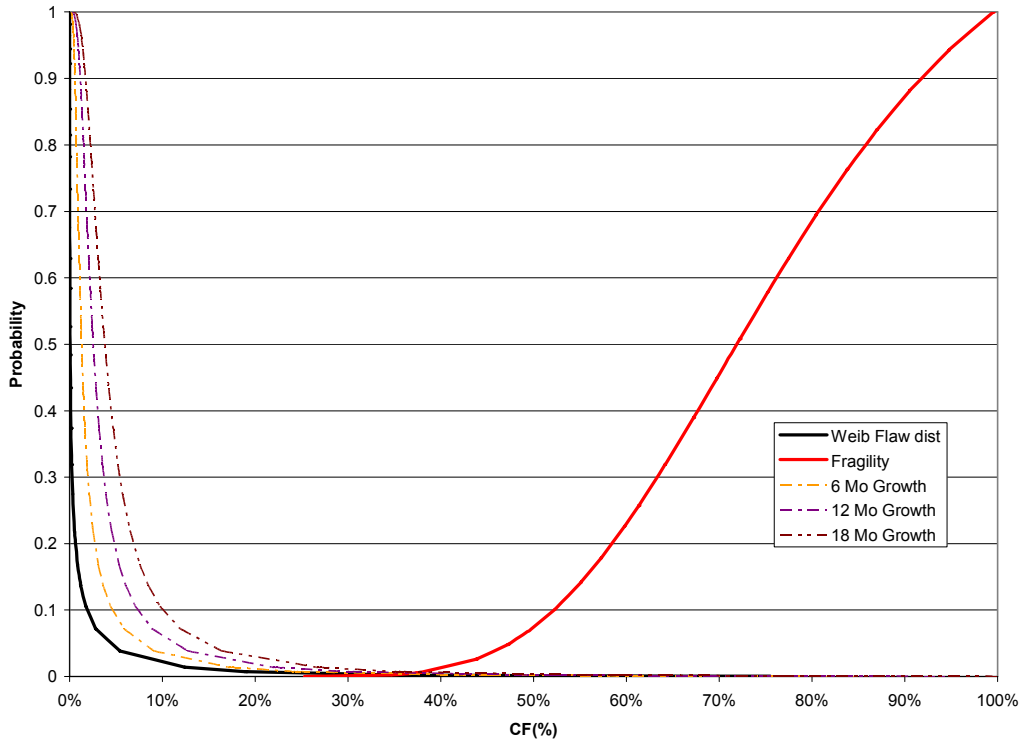
1. Flaw Distribution - As discussed in the Section 2 of this report, considering inspections performed through Spring of 2007, data exists for a total of 51 Alloy 82/182 nozzles that either have been inspected as part of the MRP-139 inspection program [2], or in which leaks, cracks or UT indications have been detected prior to the commencement of MRP-139 examinations in 2006. These data, summarized in Table 2-1, and illustrated graphically in Figure 2-1, are used to estimate probable flaw distributions that might exist in uninspected nozzles.
2. Fragility Curve - A second important aspect of the analysis, discussed in Section 3, is the critical flaw size to cause a nozzle failure. For any given flaw size, characterized in terms of percentage of cross section lost to the crack (denoted in this report as the Criticality Factor, CF%), there is a probability that the flaw will cause a pipe rupture under operating loads and internal pressure. This probability of rupture versus flaw size is called a “fragility curve” which can be combined with a probable flaw distribution to estimate the probability of a nozzle failure in the time period up to the time of the recent inspections.
3. Crack Growth – The flaw distribution discussed in 1 above represents a snapshot at the time of the inspections. In order to make meaningful comparisons of future probabilities of rupture under various inspection scenarios, one must also make estimates of the probability of future flaw growth. The deterministic results of the advanced FEA project [1] are used, as discussed in Section 4, to produce a series of flaw distributions similar to those discussed in 1 above, but which increase with time. These time-varying crack size distributions are used in conjunction with the fragility curve to produce estimates of the probability of rupture versus time into the future (at six month intervals).

The analysis process is illustrated in Figure 1-1. A typical flaw distribution (Weibull) at the time of the recent inspections is illustrated by the heavy black curve on the left hand side of the graph. This curve is estimated to shift to the right due to crack growth during each six-month period between outage seasons, as illustrated by the series of parallel colored curves in the figure. Finally, the fragility curve is illustrated by the heavy red curve, on the right hand side of the figure. Figure 1-1b zooms in on the low probability region of the same graph.

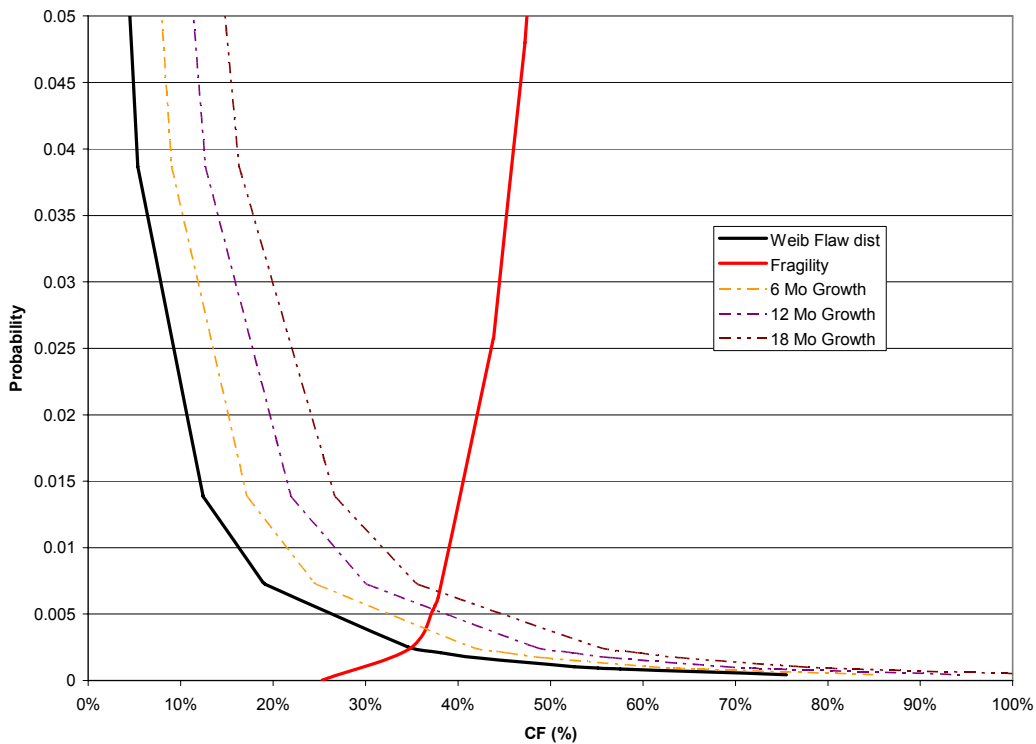
DRAFT

1 The failure probability is actually simulated by a process of Monte Carlo sampling from a
2 flaw distribution and the fragility curve, as discussed in detail in Section 5. Each time a
3 trial yields a flaw size from the flaw distribution that is greater than the critical flaw size
4 from the fragility curve; it represents a predicted nozzle rupture. The number of
5 predicted ruptures divided by the total number of trials performed represents the
6 cumulative probability of rupture (per nozzle) up to the time of the flaw distribution. The
7 Monte Carlo simulation process is performed for each time period for which a flaw
8 distribution has been determined, and the incremental probabilities of failure (per nozzle,
9 per time interval) are computed by subtracting the cumulative probabilities for adjacent
10 time intervals. Finally, the incremental probabilities are multiplied by the number of
11 nozzles, divided by the number of plants, and then combined by calendar year to produce
12 the common units of probability per plant year for various inspection scenarios.

DRAFT



1
2 **Figure 1-1a – Complementary Cumulative Distribution of Crack Area Fraction**
3 **at Different Times, along with Complementary Cumulative Distribution of**
4 **Critical Crack Area Fraction (CF, %)**



5
6 **Figure 1-1b – Enlargement of Low Probability Region of Figure 1-1a.**

DRAFT

2 Flaw Distributions

The flaw size distribution is estimated from inspection data.

2.1 Inspection Data

A compilation of the inspection data used to develop the flaw distributions is provided in Table 2-1. There are a total of 51 data points listed, in approximate chronological order, with a total of 7 axial indications (or leaks), and 8 circumferential indications. The early data (2005 and earlier) are legacy data that preceded MRP-139 inspections, and in some cases include non-pressurizer nozzles such as hot and cold leg drains, as well as overseas plants. The 2006 and 2007 data are from inspections performed in response to MRP-139. The circumferential indications include the three Wolf Creek indications observed in Fall-2006.

The data were updated to reflect recent inspections performed in Spring 2007. These include a total of ten new data points, nine clean and one moderate-sized circumferential indication. These new data did not indicate any new trends that weren't apparent from the prior data.

Figure 2-1 presents a locus plot of the data in which crack length as a percentage of circumference is plotted along the abscissa, and crack depth as a percentage of thickness on the ordinate. Axial indications plot along the vertical axis ($l/\text{circumference} = 0$) in this plot, with leaking flaws plotted at $a/t = 100\%$. Circumferential indications plot at non-zero values of $l/\text{circumference}$, at the appropriate a/t . Clean inspections are plotted randomly in a 10% box near the origin, to give some indication of inspection uncertainty.

Also shown on this plot are loci of critical flaw sizes from the fragility curve discussion in Section 3. 50th and 99.9th percentile plots are shown. It is seen from this figure that all of the flaw indications detected were far short of the sizes needed to cause a rupture. However, the analysis must address the small but finite probability that larger flaws may exist in uninspected nozzles, plus the potential for crack growth during future operating time until all the nozzles are inspected (or mitigated).

There exist a total of about 280 Alloy 82/182 pressurizer nozzles in 50 PWRs affected by this concern. Under the industry inspection program in accordance with MRP-139 (and approved deviations) 83 nozzles were inspected or mitigated, by the end of 2006, at the time that the Wolf Creek indications were observed. An additional 74 were performed in Spring 2007, and 70 are scheduled for Fall 2007. (Note that many of the nozzles were preemptively overlaid without inspection prior to the overlay, and the post-overlay inspections cover a limited volume, explaining why the numbers of inspections in Table 2-1 are much less than these totals.) The issue being addressed in this report, and the advanced FEA project of [1] concerns a total of 51 nozzles in 9 plants for which inspections or mitigation will not be performed until Spring 2008 under the industry program.

DRAFT

1

Table 2-1 – Plant Data used in Flaw Distribution

Plant	Inspection Date	Nozzle	OD (in)	Thick (t, in)	Type of Indication	Indication Depth (a, in)	Indication Length (ℓ in)	a/t	ℓ/circ	Criticality Factor
Tihange 2	2002	Surge	14	1.4	Axial	0.600	0.000	43%	0%	0.00%
TMI	2003	Surge	12	1.3	Axial	0.585	0.000	45%	0%	0.00%
Tsuruga	2003	Relief	6	1	Axial	1.000	0.000	100%	0%	0.00%
Tsuruga	2003	Safety	6	1	Axial	0.900	0.000	90%	0%	0.00%
Calvert 2	2005	CL Drain	2	0.56	Circ	0.056	0.628	10%	10%	1.00%
Calvert 2	2005	HL Drain	2	0.56	Axial	0.392	0.000	70%	0%	0.00%
DC Cook	2005	Safety	8	1.4	Axial	1.232	0.000	88%	0%	0.00%
Farley 2	2005	Safety	8	1.1	Clean	0.000	0.000	0%	0%	0.00%
Farley 2	2005	Spray	6	0.83	Clean	0.000	0.000	0%	0%	0.00%
Millstone 3	2005	Spray	6	0.9	Circ	0.220	3.750	24%	20%	4.86%
Calvert 1	2006	HL Drain	2.875	0.375	Circ	0.100	0.450	27%	5%	1.33%
Calvert 1	2006	Relief	6.0675	1.3	Axial	0.100	0.000	8%	0%	0.00%
Calvert 1	2006	Surge	12.75	1.3	Circ	0.400	2.400	31%	6%	1.84%
Davis Besse	2006	CL Drain	2	0.56	Axial	0.056	0.000	7%	0%	0.00%
D-B	2006	Relief	4.5	0.8125	Clean	0.000	0.000	0%	0%	0.00%
D-B	2006	Safety	4.5	0.8125	Clean	0.000	0.000	0%	0%	0.00%
D-B	2006	Safety	4.5	0.8125	Clean	0.000	0.000	0%	0%	0.00%
D-B	2006	Spray	5.125	0.625	Clean	0.000	0.000	0%	0%	0.00%
D-B	2006	Surge	11.5	1.125	Clean	0.000	0.000	0%	0%	0.00%
Prairie Is.	2006	Surge	15	1.5	Clean	0.000	0.000	0%	0%	0.00%
SONGS 2	2006	Safety	8	1.4	Axial	0.420	0.000	30%	0%	0.00%
SONGS 2	2006	Safety	8	1.4	Axial	0.420	0.000	30%	0%	0.00%
SONGS 2	2006	Safety	8	1.4	Clean	0.000	0.000	0%	0%	0.00%
SONGS 2	2006	Spray	5.5	0.75	Clean	0.000	0.000	0%	0%	0.00%
SONGS 3	2006	Relief	8	1.1875	Clean	0.000	0.000	0%	0%	0.00%
SONGS 3	2006	Safety	8	1.1875	Clean	0.000	0.000	0%	0%	0.00%
SONGS 3	2006	Safety	8	1.1875	Clean	0.000	0.000	0%	0%	0.00%
SONGS 3	2006	Spray	5.5	0.75	Clean	0.000	0.000	0%	0%	0.00%
SONGS 3	2006	Surge	13	1.437	Clean	0.000	0.000	0%	0%	0.00%
Watts Bar	2006	Relief	7.75	1.29	Clean	0.000	0.000	0%	0%	0.00%
Watts Bar	2006	Safety	7.75	1.29	Clean	0.000	0.000	0%	0%	0.00%
Watts Bar	2006	Safety	7.75	1.29	Clean	0.000	0.000	0%	0%	0.00%
Watts Bar	2006	Safety	7.75	1.29	Clean	0.000	0.000	0%	0%	0.00%
Watts Bar	2006	Spray	6	0.9	Clean	0.000	0.000	0%	0%	0.00%
Watts Bar	2006	Surge	15	1.5	Clean	0.000	0.000	0%	0%	0.00%
Wolf Creek	2006	Relief	7.96	1.32	Circ	0.340	11.500	25.8%	46%	11.85%
Wolf Creek	2006	Safety	7.96	1.32	Circ	0.297	2.500	22.5%	10%	2.25%
Wolf Creek	2006	Safety	7.96	1.32	Clean	0.000	0.000	0%	0%	0.00%
Wolf Creek	2006	Safety	7.96	1.32	Clean	0.000	0.000	0%	0%	0.00%
Wolf Creek	2006	Spray	6	0.9	Clean	0.000	0.000	0%	0%	0.00%
Wolf Creek	2006	Surge	15	1.45	Circ	0.465	8.750	32.1%	19%	5.95%
Farley 2	2007	Safety	8	1.1	Clean	0.000	0.000	0%	0%	0.00%
Farley 2	2007	Safety	8	1.1	Clean	0.000	0.000	0%	0%	0.00%
Farley 2	2007	Safety	8	1.1	Clean	0.000	0.000	0%	0%	0.00%
Farley 2	2007	Safety	8	1.1	Clean	0.000	0.000	0%	0%	0.00%
Farley 2	2007	Spray	6	0.83	Clean	0.000	0.000	0%	0%	0.00%
Farley 2	2007	Surge	15	1.52	Circ	0.500	3.000	33%	6%	2.12%
Calvert 2	2007	Safety	8	1.1875	Clean	0.117	1.886	0%	0%	0.00%
Calvert 2	2007	Safety	8	1.1875	Clean	0.052	1.681	0%	0%	0.00%
Calvert 2	2007	Spray	5.5	0.75	Clean	0.066	1.475	0%	0%	0.00%
Calvert 2	2007	Surge	13	1.437	Clean	0.030	3.107	0%	0%	0.00%

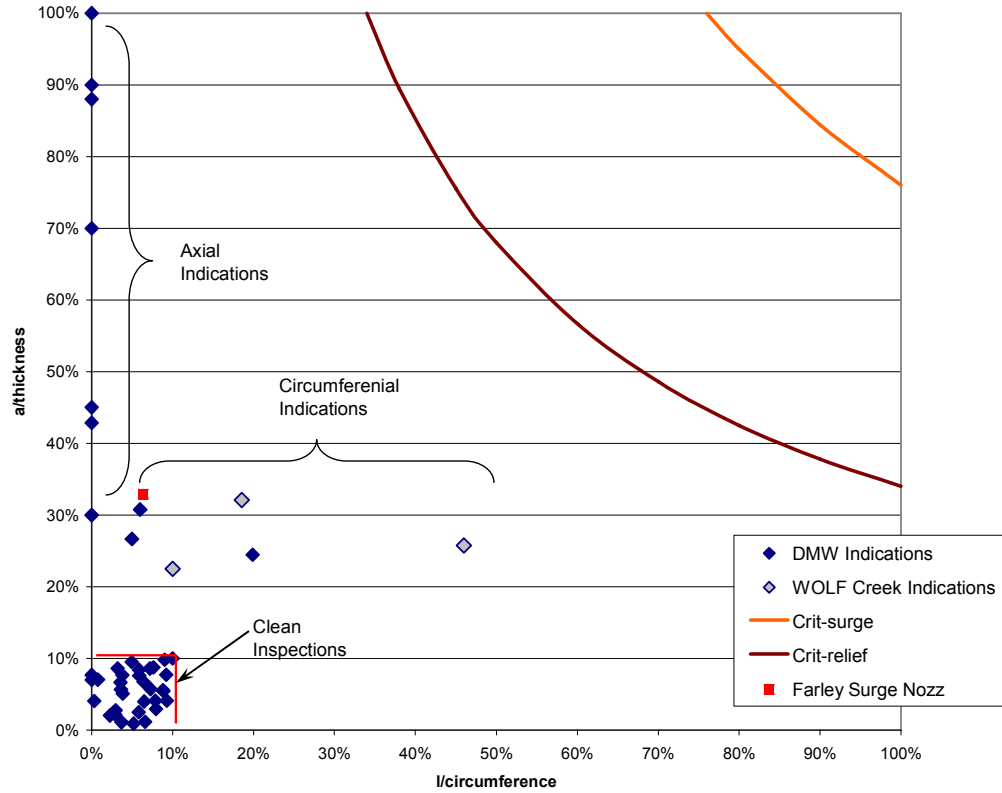
2

3

4

5

DRAFT



1
2
3
4

Figure 2-1: Plot of Indication Sizes along with 50th and 99.9th Percentiles of Fragility Curve.

2.2 Statistical Fits to the Data

5
6
7
8
9
10
11
12
13
14
15
16
17
18
19
20
21
22
23

The “Criticality Factor” (CF = percentage of cross section lost to the assumed crack) was computed for each of the nozzles in Table 2-1 (last column), by multiplying the reported indication circumferential lengths times their depths, and dividing the product by the approximate cross sectional area of the nozzle at the flaw location. CF corresponds, approximately, to the percentage of circumferential cross sectional area that is lost due to the observed indications, assuming that they are cracks with a depth equal to their maximum reported depth over the entire length of the indication. A cumulative distribution of criticality factors was then developed, by sorting the data from smallest to largest CF and assigning each data point a rank of i/N (where i = the inverse rank of each data point and N = the total number of data points, 51). The individual data points are listed in Table 2-2, which also shows the estimated cumulative probability (i/N) of an indication exceeding each CF value. Note that Table 2-2 only lists the eight nozzles that had circumferential indications. The other 43 nozzles had a CF of zero (clean or axial indications only) and were not included in curve fitting the distribution, although N was assigned as the total number of data points (51).

DRAFT

Table 2-2: Axial Indications from Table 2-1 Including Estimates of Cumulative Probability

	CF	Rank, i	F, i/N*	1-F
	1.00%	8	0.156863	0.843137
	1.33%	7	0.137255	0.862745
	1.84%	6	0.117647	0.882353
	2.09%	5	0.098039	0.901961
	2.25%	4	0.078431	0.921569
	4.86%	3	0.058824	0.941176
	5.95%	2	0.039216	0.960784
* N = 51	11.85%	1	0.019608	0.980392

Weibull, Log-Normal and Exponential fits to the data of Table 2-2 are shown on a log-log scale in Figure 2-2. The fits to the data were made by fitting a straight line to the data after transforming it to scales that would result in a straight line if the random variable had that distribution (equivalent to plotting it on probability paper appropriate for each distribution type). The resulting distributions and the data are shown in Figure 2-2. Table 2-3 summarizes the parameters of the fits.

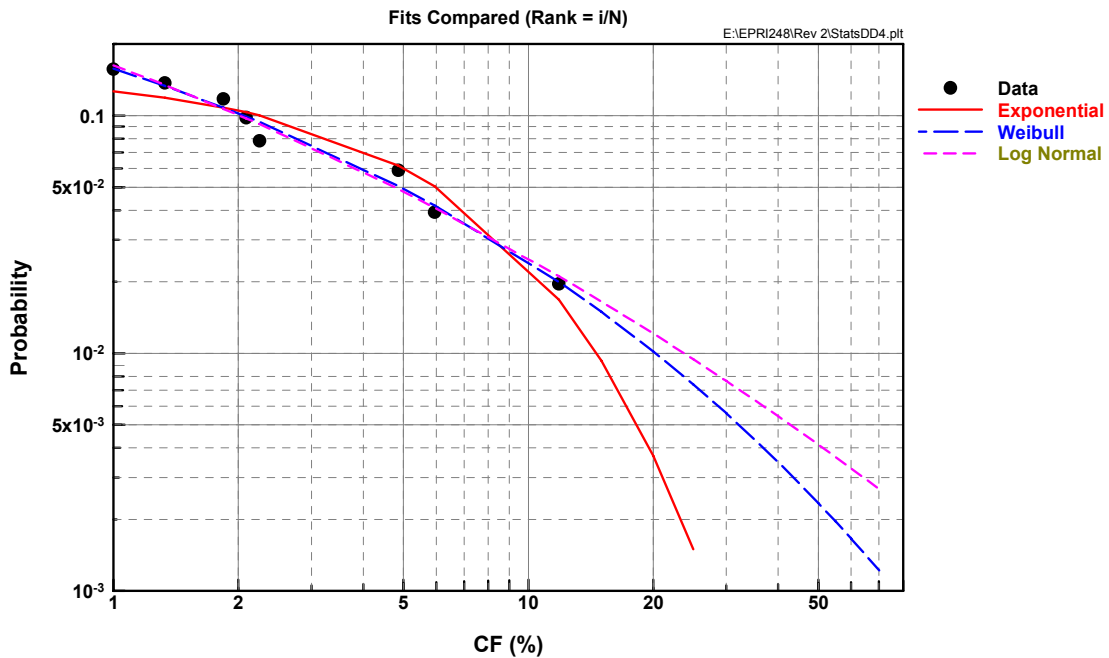


Figure 2-2 – Complementary Cumulative Distributions of CF showing each of the Three Fits along with the Data.

DRAFT

1
2
3
4

Table 2-3 - Parameters of the Fitted Distributions

Distribution Type	Complementary Cumulative Distribution	Values of Parameters	R²
Exponential	$Ce^{-x/b}$	$1/b = 18.608,$ $C = 0.1524$	0.9349
Weibull	$e^{-(x/\eta)^\beta}$	$\beta = 0.3034,$ $\eta = 0.001321$	0.9772
Log-Normal	$\frac{1}{2} \operatorname{erfc} \left[\frac{\ln(x/m)}{\sigma\sqrt{2}} \right]$	$m = 0.0009785,$ $\sigma = 2.36058$	0.9765

5
6
7
8
9
10
11
12
13
14
15
16

From Figure 2-2 it is seen that the Weibull and Log-Normal distributions are excellent fits within the range of the actual data (up to ~12% CF). The exponential distribution fit is not as good, but still reasonable. Figure 2-2 also shows the distributions extrapolated out to large flaw sizes, from which it is seen that there are substantial differences between the distributions at large sizes, even though they all agree well in the range of the data. For this reason, the probabilistic analysis will not be used to estimate absolute failure probabilities, but rather to compare relative probabilities for various inspection scenarios, under a common set of assumptions. Results of Monte Carlo simulations for the three distribution types are presented in Section 5.

DRAFT

1

2 **3 Critical Flaw Size Distribution**

3

4 There are two sources of statistical variability in the critical flaw size calculations. One is
5 the variability in the applied loads for the different plants and nozzle types, and the
6 second relates to uncertainty in ability to predict critical flaw size (CF%) when the
7 applied loading is known. These two sources of variability are addressed separately and
8 then combined statistically to produce a single fragility curve as discussed in the
9 following subsections.

10 **3.1 Applied Load Distribution**

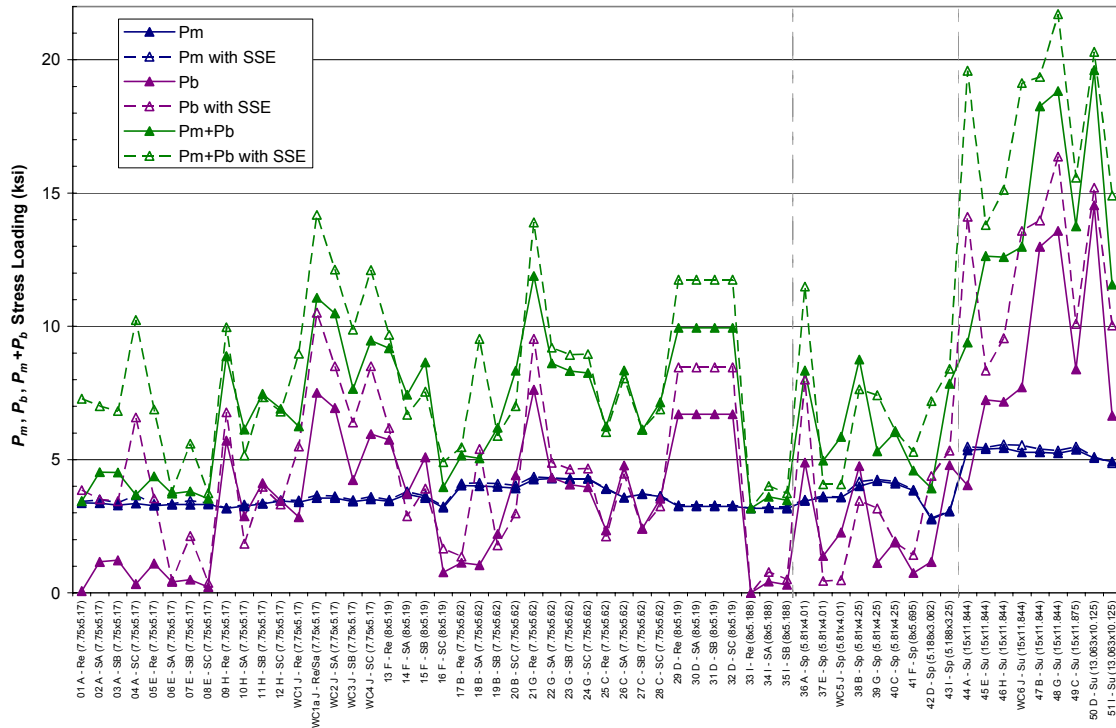
11 Applied loads for the 51 PWR pressurizer nozzles scheduled for Spring 2008 inspections,
12 plus the Wolf Creek pressurizer nozzles, have been compiled as part of the advanced
13 FEA project [1]. Figure 3-1 presents a summary of this compilation, in terms of ASME
14 Code membrane and bending stress levels (Pm and Pb) computed using standard Code
15 formulas and nozzle dimensions for each plant. The loads include pressure and dead
16 weight primary loading plus sustained thermal expansion (Pe) loads, which are secondary
17 or displacement controlled. Thermal stratification loads, which are also secondary, are
18 not included. Analyses were performed in the advanced FEA project [1] which
19 demonstrate that secondary loads do not need to be included in critical flaw size
20 computations for the ductile Alloy 82/182 weld materials being addressed in these
21 nozzles, thus justifying the exclusion of both thermal expansion and stratification loads.
22 However, an agreement was reached under the project to include sustained thermal
23 expansion loads in the critical flaw size computations, since they are used to support leak
24 rate predictions. For consistency these thermal expansion loads are also included in
25 critical flaw size calculations performed for the probabilistic evaluation.

26

27 Safe shutdown earthquake (SSE) loads are also included in Figure 3-1, as indicated by
28 the dashed lines in the plot. For the probabilistic evaluation, the load data were analyzed
29 separately, with and without SSE loads, permitting seismic loads to be considered with a
30 reduced probability of occurrence (typically 0.001 per year or less) relative to normal
31 operating loads.

32

DRAFT

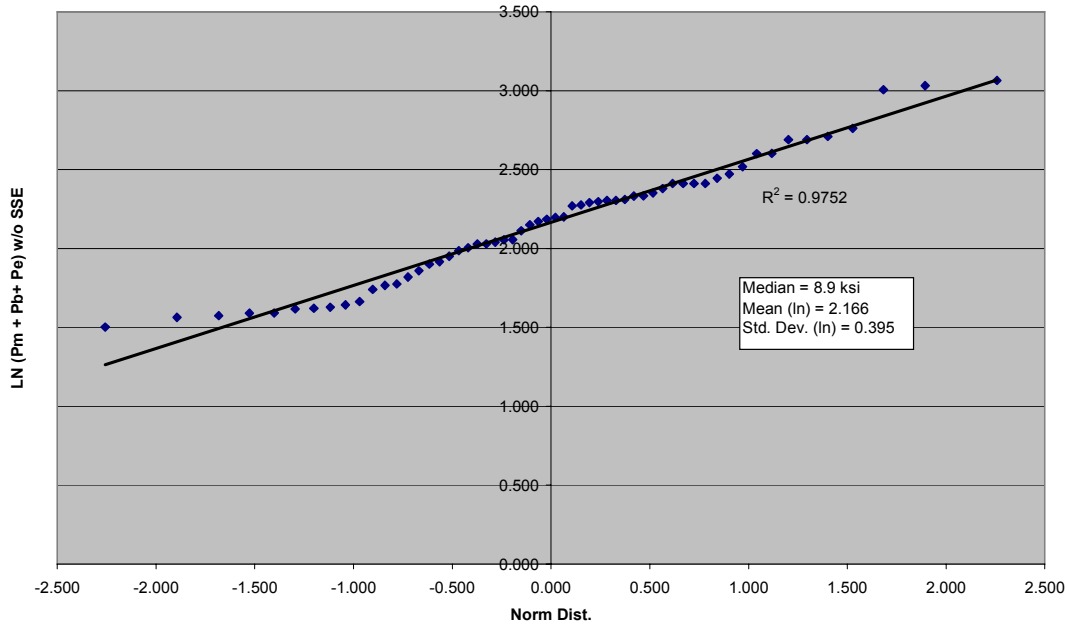


1
2 **Figure 3-1 – Compilation of Applied Stresses (Pm + Pb + Thermal Expansion) in 51**
3 **Pressurizer Nozzles scheduled for Spring 2008 Inspection plus Wolf Creek**

4
5
6
7 The data in Figure 3-1 were sorted by increasing stress level, and were found to be well
8 fit by Log-Normal statistical distributions, as illustrated in Figures 3-2 and 3-3 for Pm +
9 Pb + Pe, with and without SSE loads, respectively. The fitting accuracy and parameters
10 of the Log-normal fits are included on the figures.

DRAFT

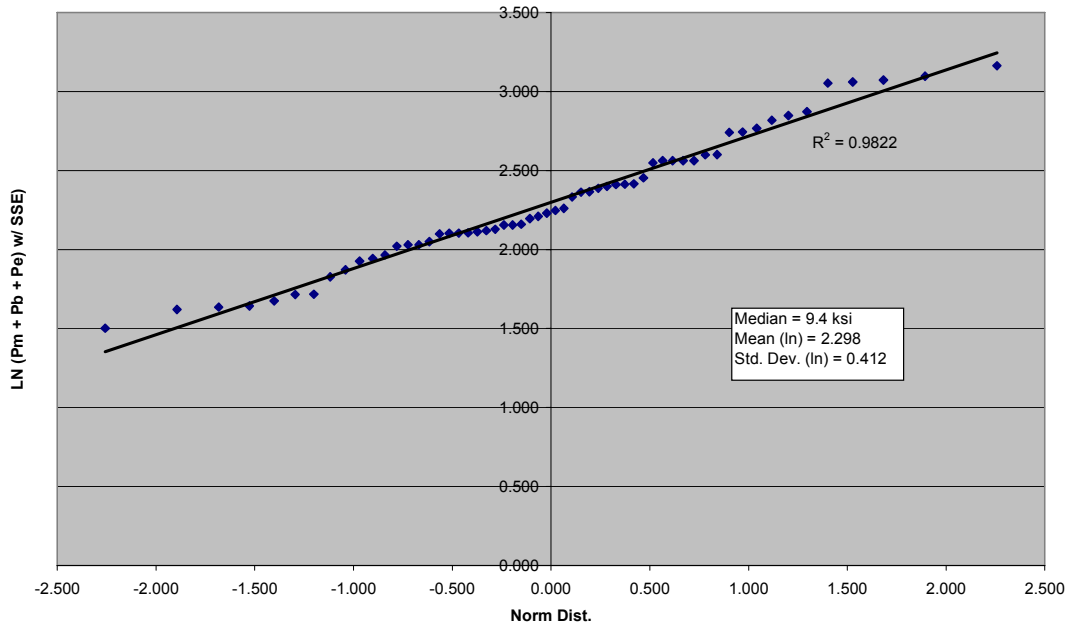
Log Norm Fit (w/o SSE)



1
2
3
4

Figure 3-2 – Log-normal Fit and Parameters of Applied Load Distribution without Seismic Loads

Log Normal Fit w/SSE



5
6
7
8

Figure 3-3 - Log-normal Fit and Parameters of Applied Load Distribution without Seismic Loads

DRAFT

3.2 Compilation of Full Scale Pipe Tests

The statistical fits of figures 3-2 and 3-3 can be sampled to provide estimates of the distribution of applied loading on the pressurizer nozzles in the study. However, even if the applied loading were known with complete accuracy, uncertainty exists in our ability to predict the critical flaw size, in terms of CF%. To help characterize this uncertainty, a review was performed of test data from the NRC-sponsored Degraded Piping Program conducted at Battelle Columbus Laboratories [3, 4]. Approximately 60 full scale pipe tests were conducted in this program, of pipes containing three types of circumferential defects: through-wall cracks, surface cracks, and complex cracks (see Figure 3-4). Pipe sizes ranged from 4" to 42" and loadings included 4-point bending, combined bending + internal pressure and pure axial load. The majority of the pipes tested were in the 6" to 16" range which is directly relevant to the pressurizer nozzles being evaluated. Pipe materials in the tests included 304 stainless steel, Alloy 600 and Carbon Steel, but no pipes containing A-82 or 182 weldments were tested. Therefore the results of the predominantly base material pipe tests must be translated to DMWs on the basis of relative material properties for use in this evaluation. Fortunately, the piping materials used in the program were extensively characterized in terms of tensile properties and fracture toughness (J-R curves). Recent data also exists on the J-R properties of a large A-182 weldment, which can be used for comparison to the test materials.

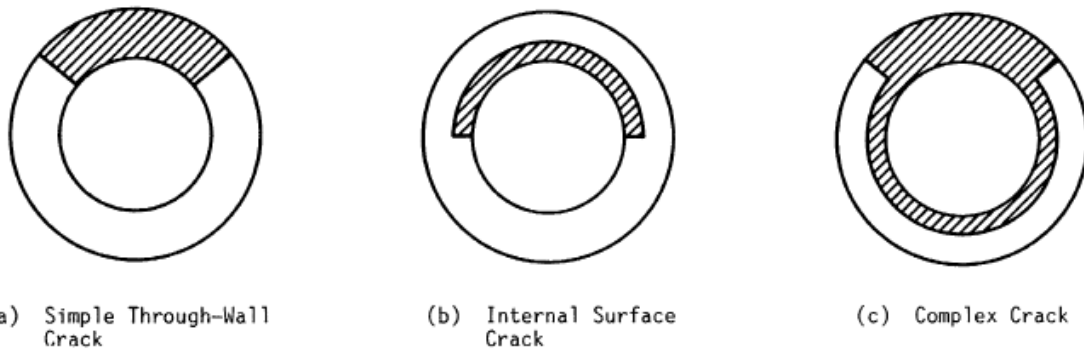
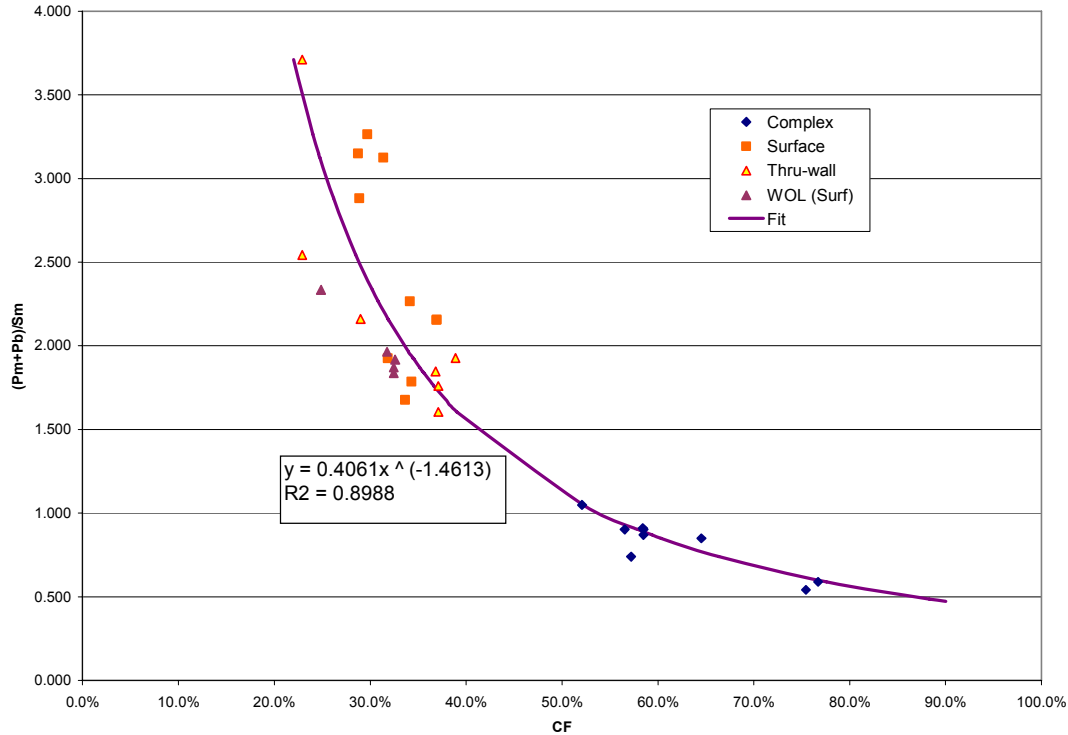


Figure 3-4 – Illustration of Circumferential Flaw Types Tested in Degraded Piping Program Full Scale Pipe Tests

Figure 3-5 is a plot of test data from 31 of the pipe tests, performed on Austenitic materials only (304SS plus A-600). The data are plotted in terms of maximum loading achieved in the pipe tests (i.e. failure load) vs. % of pipe cross section cracked (CF %). The maximum load is plotted in terms of applied stress at the cracked cross section normalized by the ASME Section III design allowable stress for the appropriate material and temperature: $(P_m + P_b) / S_m$.

DRAFT



1
2 **Figure 3-5 – Plot of Full Scale Pipe Test Data from Degraded Piping Program.**
3 **Austenitic Materials Only; Various Flaw Types,**

4
5
6 The large majority of the tests in Figure 3-5 were conducted under bending loading (Pb)
7 only, and those tests yielded a very consistent trend. However, in order to include pipes
8 tested under combined membrane plus bending (Pm + Pb), and since the applied nozzle
9 loadings in Section 3.1 include both membrane and bending loads, a correction factor
10 was developed based on net section collapse analyses plus data from similar pipes tested
11 under varying amounts of membrane and bending stress. It results in a correction of the
12 form:

13
14
$$(Pm + Pb)/Sm_{adjusted} = [(Pm + Pb)/Sm] \times [0.9817 + 0.4311 \times Pm/(Pm + Pb)]$$

15
16 which varies from ~1 for pure bending loading (Pm/(Pm + Pb) = 0) to ~1.4 for pure
17 membrane loading (Pm/(Pm + Pb) = 1).

18
19 Plotting the test results in this manner yields a monotonic trend with relatively little
20 scatter, indicating that CF% is a reasonable parameter for characterization of the effect of
21 cracking on pipe failure load, at least for the configurations tested.

DRAFT

1

2 **3.3 Development of Fragility Curve**

3 Also shown on Figure 3-5 is a power law fit of the data:

4

5

$$(Pm + Pb)/Sm = 0.4061 (CF)^{-1.4613}$$

6

7 In order to develop a statistical distribution for this curve, residuals were calculated based

8 on the difference between the actual CF for each data point and that predicted by the

9 power law fit ($CF - CF_{\text{predicted}}$). The residuals were then sorted from lowest to highest,

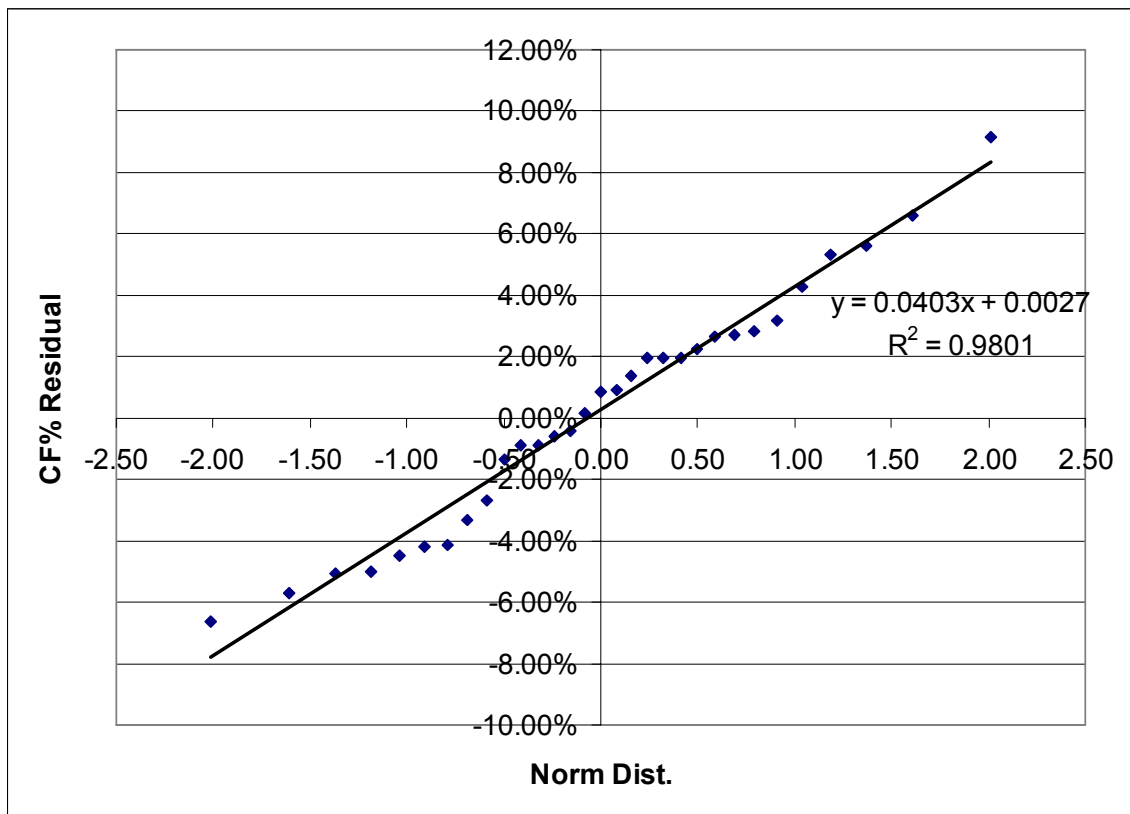
10 and were found to be reasonably represented by a normal distribution, as illustrated in

11 Figure 3-6. CF% was selected as the dependent variable in this correlation, since applied

12 loading is the independent variable in the analysis (i.e. applied loads determined from the

13 plant loading distributions are used to determine critical CF% from Figures 3-5 and 3-6).

14



15

16 **Figure 3-6 – Normal Probability Plot of the CF% Residuals between Test Data and**
17 **Power-Law Curve in Figure 3-5**

18

19 Consistent with the advanced FEA project, the applied loads are first multiplied by a Z-

20 factor [5] before entering Figures 3-5 and 3-6 which accounts for potentially lower

21 toughness of Alloy-182 weldments relative to the austenitic base materials tested in the

22 pipe tests. J-Resistance testing of a typical Alloy-182 weldment showed little or no

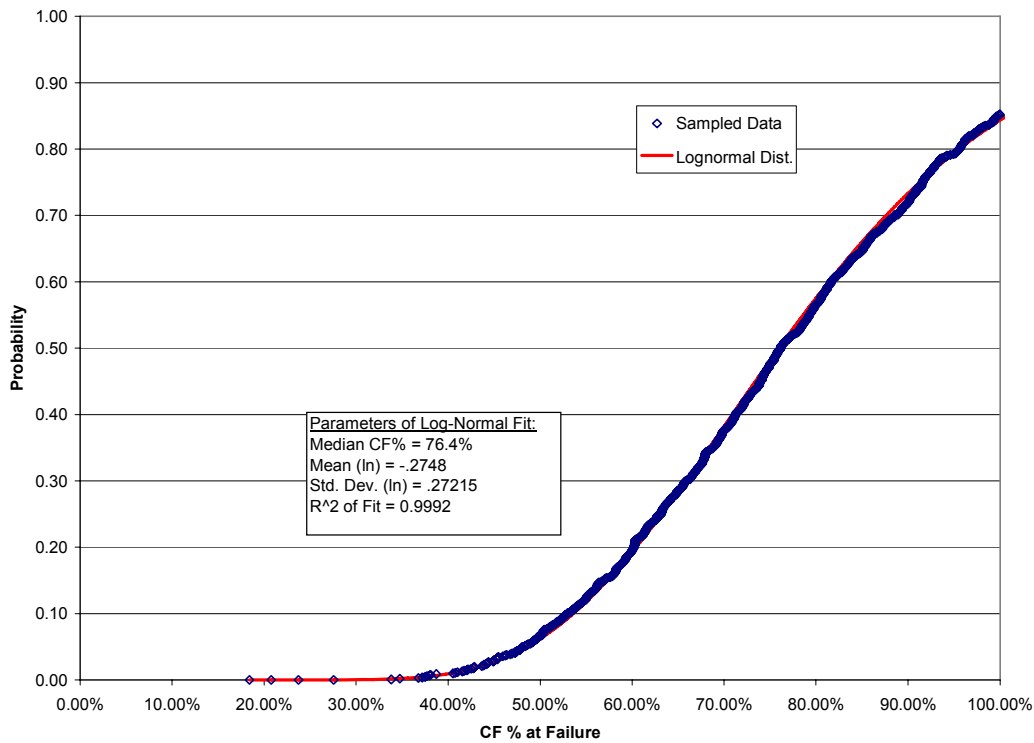
23 reduction in toughness relative to the pipe test materials [5]. Sm for stainless steel base

24 metal at pressurizer operating temperature was used to normalize the plant loads.

DRAFT

1
2
3
4
5
6
7
8
9
10
11
12
13

The final step in developing the fragility curve was to perform Monte Carlo sampling from the load distribution of Figure 3-2, and then independently sample the critical flaw size distribution of Figures 3-5 and 3-6 for critical CF % for each load. Consideration was given to occasionally sampling from the SSE distribution of Figure 3-3 (e.g. once in every 1000 simulations), however, the two distributions are so close that this was judged to have an insignificant effect. 1000 samples were performed, resulting in the critical flaw size distribution shown in Figure 3-7. Both the sampling results and a Log-Normal fit to the distribution are plotted. The Log-Normal fit was found to give a very accurate representation of the fragility curve distribution. Parameters of the Log-Normal fit are also listed in Figure 3-7.



14
15
16
17
18
19
20
21
22
23
24

Figure 3-7 – Resulting Fragility Curve and Associated Log-Normal Fit

One anomaly exists in the fragility curve in Figure 3-7: it yields a probability of failure of less than one for CF = 100%, which is physically impossible. This effect results from sampling the tails of the two distributions, which occasionally yields unrealistically small applied loads or unrealistically high critical flaw sizes (For example, the right hand side of the power law curve in Figure 3-5 doesn't go through zero.) However, this anomaly is corrected in the Monte Carlo analyses of Section 5 by discarding and re-sampling any trials in which the critical flaw size is predicted to be greater than 100%.

DRAFT

1

2 **4 Crack Growth**

3

4 **4.1 Summary of Advanced FEA Results**

5 The advanced FEA analyses addressed a total of 53 cases with variations of each
6 resulting in over 100 individual crack growth analyses. Over half of the analyses
7 demonstrated stable crack arrest prior to penetrating through-wall or reaching critical
8 size,. The remainder exhibited varying degrees of crack growth. The first 20 cases were
9 denoted base cases, and include cases that envelope all geometries and loads for the 51
10 Spring 2008 pressurizer nozzles. The 20 base cases and their resulting crack growth
11 rates, in terms of CF% per year are summarized in Table 4-1. (Note that a total of 22
12 analyses are actually reported in the table since two cases were run with two sets of weld
13 residual stresses each.) The crack growth rates naturally divide into two regimes: crack
14 growth from initial assumed flaw size until through wall (TW) penetration, denoted
15 “Rate1” in the table, and crack growth following TW penetration, denoted “Rate2”.
16 Rate2 can be seen to be on average about an order of magnitude greater than Rate1,
17 indicating significant acceleration in crack growth once the assumed crack breaks
18 through and becomes through wall.

19

20 Another observation from Table 4-1 is that all but two base cases exhibit relatively small
21 pre-TW crack growth rates ($\sim 1\%/yr < \text{Rate1} < 3.5\%/yr$) with the exception of Case 6
22 ($9.85\%/yr$) and Case 17 ($14.97\%/yr$). A similar trend is seen in the post-TW growth rates
23 (Rate2), albeit at much higher rates. Thus for the geometries enveloped, the high crack
24 growth rates predicted for cases 6 and 17 are relatively rare. The remainder of the cases
25 (21 through 53) for the most part started with cases 6 and 17 and looked at the effect of
26 various analysis parameters and assumptions on these bounding cases. For this reason, it
27 was judged not appropriate to include these remaining cases in the statistical distribution
28 of crack growth rates, since they would bias the distribution very much to the high side.
29 Instead, only the base cases were used, but the spread in the distributions was combined
30 with the experimental scatter in crack growth rates from MRP-115 [6], as described in the
31 next section.

32

DRAFT

Table 4-1 – Summary of Base Case Crack Growth Results from Advanced FEA Project [1]

Case Number	Nozzle Type	CF% Initial	CF% @ TW	Time to TW (yrs)	Rate1 CF%/yr	CF% @ 1GPM	Time (days)	Time to 1 GPM (yrs)	CF% @ LF =1.2	Time (yrs)	Comb Time (yrs)	Rate2 CF%/yr
1	S&R	10.00%	40.00%	17.4	1.72%	46.60%	114	0.312	56.80%	0.299	0.611	27.50%
2	S&R	10.00%	39.50%	21.3	1.38%	47.00%	142	0.389	57.40%	0.323	0.712	25.13%
3	S&R	10.00%	38.30%	26.3	1.08%	47.20%	182	0.499	58.00%	0.342	0.841	23.42%
4	S&R	10.00%	40.00%	18	1.67%	46.20%	107	0.293	55.80%	0.307	0.600	26.33%
5	S&R	10.00%	38.10%	25.7	1.09%	46.60%	180	0.493	57.40%	0.375	0.868	22.22%
6	S&R	10.00%	43.50%	3.4	9.85%	47.10%	31	0.085	52.90%	0.112	0.197	47.65%
7	S&R	10.00%	44.00%	10.5	3.24%	49.10%	70	0.192	57.30%	0.195	0.386	34.43%
8	S&R	10.00%	39.90%	13.4	2.23%	45.90%	94	0.258	55.30%	0.271	0.529	29.12%
9	S&R	10.00%	36.40%	32.2	0.82%	47.00%	229	0.627	58.60%	0.395	1.022	21.72%
10	spray	10.00%	38.90%	21.2	1.36%	49.70%	195	0.534	58.20%	0.200	0.734	26.29%
11	spray	10.00%	37.80%	25.3	1.10%	50.60%	260	0.712	58.70%	0.200	0.912	22.91%
12	spray	10.00%	43.60%	10.5	3.20%	50.70%	110	0.301	57.50%	0.132	0.433	32.11%
13	spray	10.00%	42.70%	13.6	2.40%	51.20%	130	0.356	58.20%	0.148	0.504	30.75%
14	spray	Arrest										
15	spray	Arrest										
16	spray	Arrest										
17a	surge	Arrest										
17b	surge	6.03%	24.00%	1.2	14.97%	24.30%		0	33.10%	0.096	0.096	94.90%
18a	surge	Arrest										
18b	surge	10.00%	49.90%	11.5	3.47%	52.30%		0	59.10%	0.118	0.118	78.09%
19	surge	Arrest										
20	surge	Arrest										
Average		9.74%	39.77%	16.8	3.31%	46.77%		0.337	55.62%	0.234	0.571	36.17%
Std. Dev.		1.03%	5.53%	8.8	3.92%	6.55%		0.214	6.43%	0.102	0.288	21.66%
Maximum		10.00%	49.90%	32.2	14.97%	52.30%		0.712	59.10%	0.395	1.022	94.90%
Minimum		6.03%	24.00%	1.2	0.82%	24.30%		0.000	33.10%	0.096	0.096	21.72%

DRAFT

4.2 Adaptation to Probabilistic Analysis

The base case crack growth results identified in Section 4.1 were used to define statistical distributions of crack growth rates for the probabilistic analysis. Figure 4-1 presents the sorted data for pre- and post-penetration crack growth rates plotted versus cumulative probability. Bilinear fits to the data were developed for the two regions of each of the curves. These bilinear distributions properly characterize the dichotomy observed in the FEA results (i.e. about an 80% probability that the crack growth rate will be relatively small, and about a 20% probability of large crack growth rates as observed in Cases 6 and 17). The high portion of the crack growth distributions also extrapolate out to even higher crack growth rates than those predicted for Cases 6 and 17, thereby covering to some extent the remaining sensitivity cases that weren't included in the distribution.

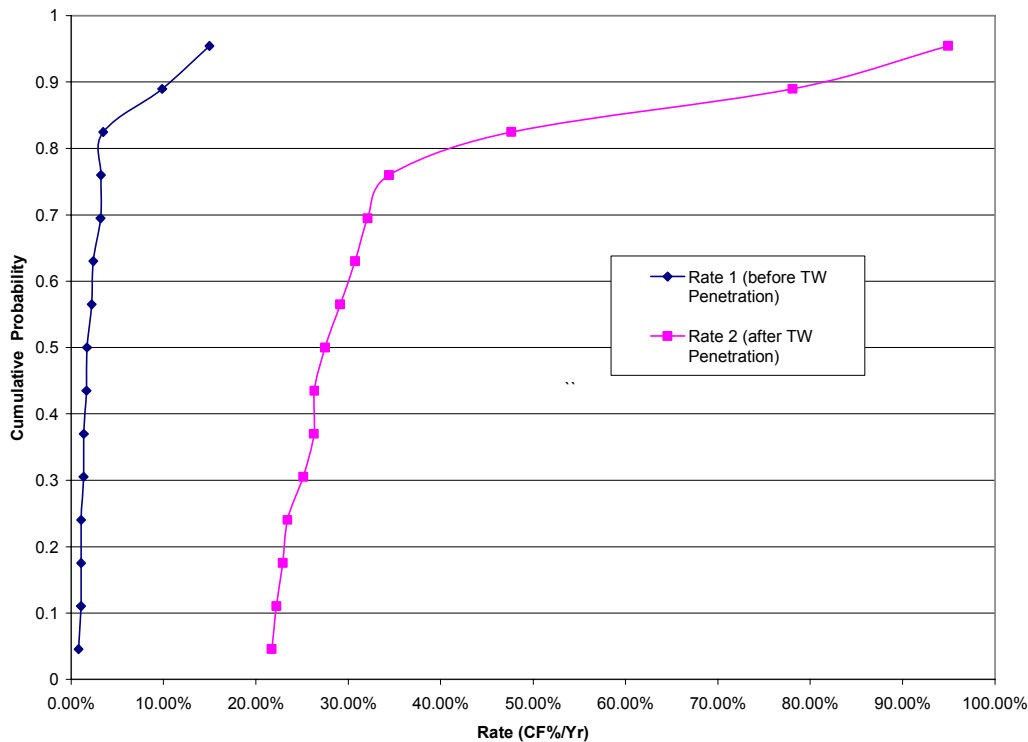


Figure 4-1: Data for Pre- and Post-penetration Area Growth Rates Illustrating the Bilinear Nature of the Distributions.

The distributions in Figure 4-1 do not include the scatter in the crack growth rate itself; All the base case computations used the 75th percentile of the MRP-155 crack growth rate distribution that describes material crack growth rate scatter (Figure 4-2).

DRAFT

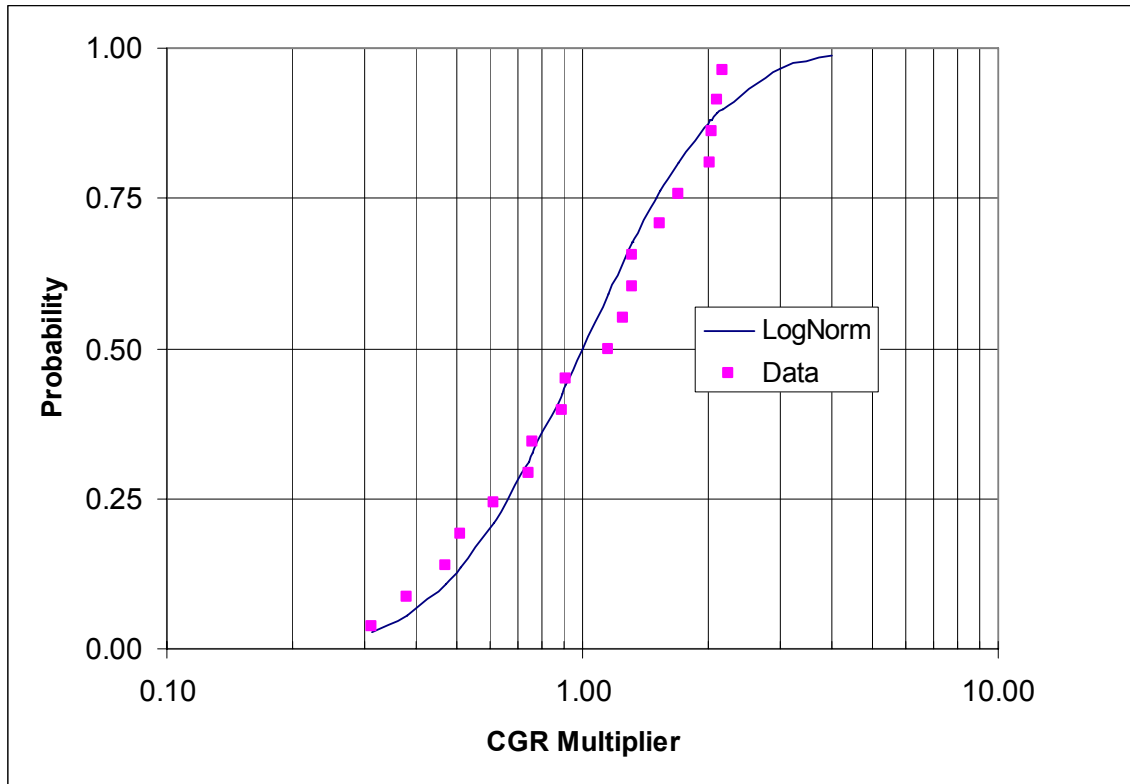


Figure 4-2 – MRP-115 Distribution Characterizing Material Crack Growth Rate Scatter for PWSCC in Alloy 182 Weld Metal

The material crack growth rate scatter needs to be combined with the above analytical distributions to obtain the overall statistical description of the crack growth rate. This was accomplished by Monte Carlo simulation employing the following steps:

1. Sample from the bilinear distributions of Figure 4-1.
2. Divide the sampled value by the ratio of the 75th to the 50th percentile of the MRP-115 distribution of Figure 4-2 (i.e. adjust to the median).
3. Sample from the MRP distribution (with a median of 1 and lognormal shape parameter of 0.6069) to determine a multiplier for the analytical crack growth rate.
4. Multiply the sample from Step 2 by the sample from Step 3.

This provides a set of samples from which a cumulative distribution can be derived. The cumulative distribution for pre-TW penetration is shown in Figure 4-3 on lognormal scales (as data points) along with a lognormal distribution that was fit to the data. The line is seen to provide a good description to the Monte Carlo results. The constants describing the line are the parameters of the lognormal distribution of crack growth rate for pre-penetration.

DRAFT

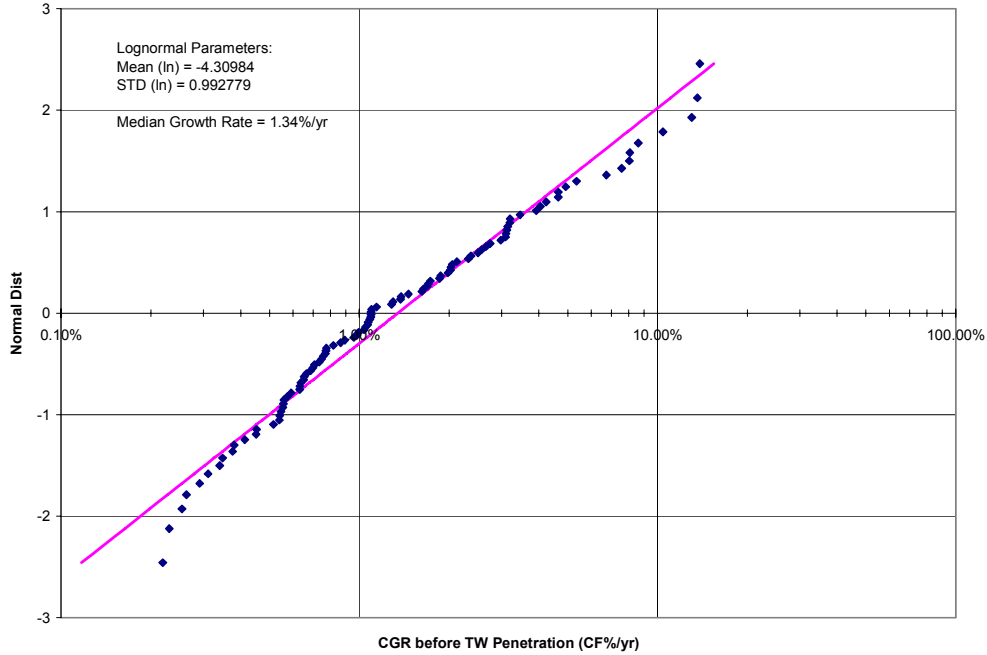


Figure 4-3: Monte Carlo Simulation Results of Pre-TW Penetration Crack Growth Rates with Fitted Lognormal Line.

A similar analysis was performed for the post-TW penetration data. Figure 4-4 provides the corresponding results.

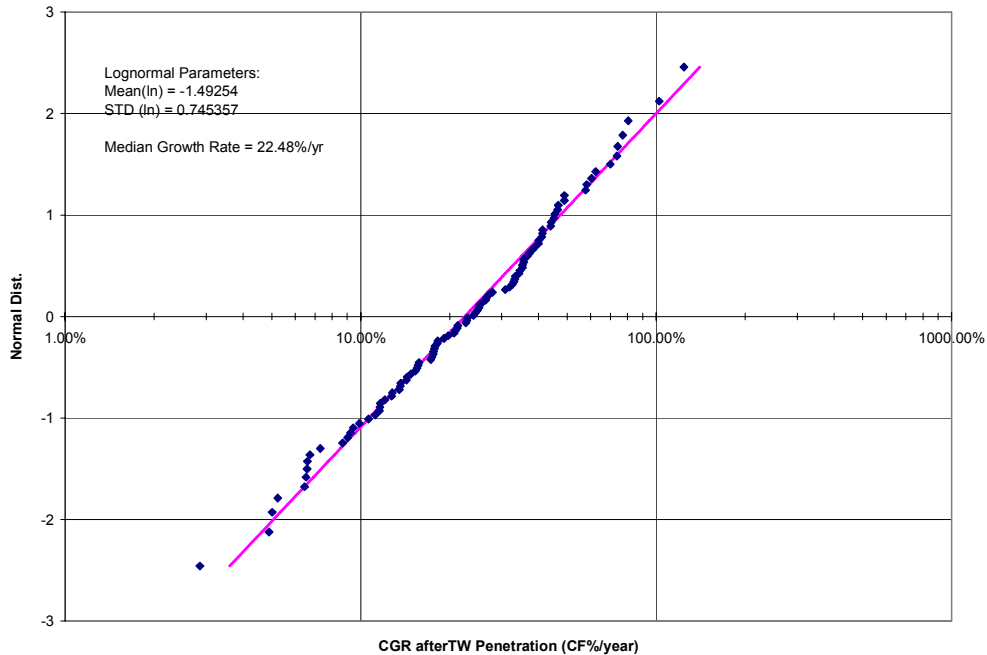


Figure 4-4: Monte Carlo Simulation of Post-TW Penetration Crack Growth Rates with Fitted Lognormal Line

DRAFT

5 Monte Carlo Analysis

Monte Carlo simulation was used to generate results of the probability of a nozzle failure as a function of time.

5.1 Methodology

The following steps were used in each trial of the Monte Carlo simulation.

1. Sample crack size (CF%) from one of the flaw size distributions (Weibull, Log-Normal, Exponential) developed in Section 2. Truncate the CF at 100% (if the sampled CF is greater than 100%, then discard it and sample again). Separate Monte Carlo analyses were conducted for each of the distribution types, and results are presented for each.
2. Sample pre-penetration crack growth rate from a log-normal distribution using the same percentile as the sampled crack size (based on the observation that the larger cracks likely were associated with high crack growth rates, either due to material, high loads, or both). This crack growth rate was used for crack sizes up to CF = 40%, which corresponds to the mean crack size at through-wall penetration in Table 4-1.
3. Sample post-penetration crack growth rate from a lognormal distribution using an independent sample. This crack growth rate was used to grow cracks beyond CF=40%.
4. Sample Fragility CF. Truncate the Fragility CF at 100% (if the sampled Fragility CF is greater than 100%, then discard it and sample again).
5. Grow the cracks in steps of 6 months at a time for up to 18 months. The pre-penetration crack growth rate is used for cracks of size less than 40%. The post-penetration crack growth rate is used once the crack size exceeds 40%. (If the initial size of the sampled crack is greater than 40 %, it will always grow at the post-penetration rate.) Failure at a given time step (0, 6, 12, 18 months) is defined as the cracking CF exceeding the fragility CF.
6. Check for crack arrest. Probability of arrest is an input, and only applies to sampled cracks of initial size that are smaller than 40% CF. If the sampled crack is less than 40%, a random sample is taken from the uniform distribution. If this sample is less than the probability of arrest, then that crack does not grow beyond 40% CF. This crack could still cause a failure if the sampled Fragility CF is less than the cracking CF. If the sampled crack size is greater than 40%, arrest is not assumed. Based on the results of the advanced FEA crack growth analyses, a probability of arrest = 0.57 was used in the Monte Carlo analyses.
7. The probability of failure is computed as the number of failures divided by the number of trials.

DRAFT

5.2 Cases Analyzed

Monte Carlo results were generated for all three distribution types (Weibull, exponential, lognormal) for times up to the present and for 6, 12, and 18 months into the future. Since the majority of the inspection data reported in Table 2-1 were from 2006, and the Wolf Creek inspection findings were observed in Fall 2006, the inspection data were treated as a snapshot in time at end of the Fall 2006 outage season, and that date was assumed to be the present, or time = 0 in the time-based probability of failure results.

5.3 Results

The results of the Monte Carlo simulations are presented in Table 5-1. 10^7 trials were used in each case. The cumulative probabilities are directly from the Monte Carlo simulation and are given for each of the three distribution-types. The incremental probabilities are the differences in the cumulative probabilities for each six-month time span. These correspond to the probability of a nozzle rupture (per nozzle) during each six-month time interval.

The number of nozzles column corresponds to the number of remaining, PWSCC-susceptible pressurizer nozzles that will not have been inspected or mitigated at the end of each outage season, assuming that the industry inspection plans are implemented. The next column reflects the number of plants containing those uninspected/unmitigated nozzles. The probability of a nozzle failure in the time increment is given by the expression $P_{noz} = 1 - (1 - p_I)^N$, where p_I is the incremental failure probability for a single nozzle and N is the number of nozzles. The per plant probability of a nozzle failure is then obtained by dividing by the number of plants in which those nozzles exist.

It may be observed from Table 5-1 that the incremental probabilities of nozzle failure are remaining about constant for each of the six month intervals, especially for the analyses performed with the Weibull and lognormal flaw distributions (which from Figure 2-1 were the better fits of the data). The analyses with the exponential distribution show some increase in incremental probability of failure versus time, but those start at much lower present values (time = 0), since the exponential fit produced less conservative extrapolations of probabilities of larger flaw sizes. Since the numbers of susceptible nozzles and plants are being removed from the population at a steady rate, the industry inspection plan results in an essentially constant probability of a nozzle failure per time interval, until the time when all nozzles will have been inspected or mitigated, at the end of the Spring 2008 outage season.

DRAFT

Table 5-1: Results of Monte Carlo Simulation

Distribution/ Outage Season	Time (months)	Time Increment (months)	Cumulative Prob.	Incremental Prob.	# Nozzles	# Plants	Nozzle Failure Probability	
							Total	per Plant
Weibull								
Fall-06	0		7.57E-04		278	50		
Spring-07	6	6	1.47E-03	7.13E-04	195	34	0.1299	0.0038
Fall-07	12	6	2.18E-03	7.09E-04	121	21	0.0822	0.0039
Spring-08	18	6	2.93E-03	7.49E-04	51	9	0.0375	0.0042
Log Normal								
Fall-06	0		1.12E-03		278	50		
Spring-07	6	6	2.03E-03	9.09E-04	195	34	0.1624	0.0048
Fall-07	12	6	2.84E-03	8.17E-04	121	21	0.0941	0.0045
Spring-08	18	6	3.60E-03	7.56E-04	51	9	0.0379	0.0042
Exponential								
Fall-06	0		5.90E-06		278	50		
Spring-07	6	6	7.03E-05	6.44E-05	195	34	0.0125	0.0004
Fall-07	12	6	2.59E-04	1.89E-04	121	21	0.0226	0.0011
Spring-08	18	6	6.58E-04	3.99E-04	51	9	0.0201	0.0022

DRAFT

6 Conclusions

The following observations are apparent from the results of the probabilistic evaluation presented in Table 5-1:

- Pressurizer nozzle failure probabilities (per plant, per six months) for the Spring-08 Plants are approximately the same as what has existed in PWRs due to PWSCC susceptible pressurizer nozzles during the Fall and Spring of 2007 (on the order of 4×10^{-3} per plant, per six months).
- The absolute failure probabilities (on the order of 8×10^{-3} per plant, per year) are greater than the generally accepted 1×10^{-3} per plant, per year. However, these results assume no leakage or plant response to leakage. For comparison to pipe break probability limits, they should be factored by the probability of non-Leak-Before-Break (or failure to react to leakage) from the advanced FEA analysis, which was shown to be very small.
- If there is just a 90% probability that leakage would be detected (i.e. a 10% or less probability that it would be missed), then the predicted failure probabilities are within the generally accepted limits. Since essentially all cases evaluated in the advanced FEA analysis demonstrated leak before break, including agreed upon margins on load, leak rate and time to failure, the probability of a significant crack/leak in one of these nozzles going undetected is considered to be much less than 10%.

Therefore, it is concluded that there is no significant risk benefit to accelerating the scheduled Spring 2008 inspections.

7 References

1. DEI Advanced FEA Program Report
2. MRP-139
3. NUREG/CR-4082, Volume 8, "Summary of Technical Results and Their Significance to Leak-Before-Break and In-Service Flaw Acceptance Criteria, March 1984- January 1989
4. Pipe Fracture Encyclopedia, U.S. NRC, 1997 (A collection of NUREG Reports and Data Files from the DP2 and other programs distributed on CDs)
5. G. Wilkowski et al, "Determination of the Elastic-Plastic Fracture Mechanics Z-Factor for Alloy 82/182 Weld Metal Flaws for Use in the ASME Section XI Appendix C Flaw Evaluation Procedures", (Draft) ASME PVP2007-26733
6. MRP-115